A Switching-less True-time-delay based Beam Probing Approach for Ultra-Low Latency Wireless Communications: System Analysis and Demonstration

Qiuyan Xu, *Graduate Student Member, IEEE,* Aditya Wadaskar, *Graduate Student Member, IEEE,* Chung-Ching Lin, *Graduate Student Member, IEEE,* Han Yan, *Member, IEEE,* Veljko Boljanovic, *Graduate Student Member, IEEE,* Subhanshu Gupta, *Senior Member, IEEE,* and Danijela Cabric, *Fellow, IEEE*

***Abstract*—Emerging wireless communication systems at millimeter-wave (mmW) require wideband phased-arrays transceivers not only for high data-rate communications but also for fast direction finding using beam training algorithms. In real world, scanning both azimuth and elevation is also important for accurate localization over three-dimensional (3D) space. This paper presents the system analysis and demonstration of frequency dispersive 3D beam training algorithm using a 2×2 planar array integrated in a single chip suited for low-latency mmW wireless communications. System-level issues with high search latency in earlier time-division based beam training algorithms and the need for multiple ICs for 3D beam training are addressed with a large delay range true-time-delay (TTD) based spatial signal processor (SSP) together with the frequency-dependent rainbow beam training algorithm. Trade-offs between angular coverage efficiency over the 3D space and required hardware delay range are analyzed. Measured results on the 2×2 antenna array demonstrate the efficacy of the 3D beam training algorithm achieving 50% spherical coverage efficiency realized with the 3.75ns IC delay range over 800MHz bandwidth.**

***Index Terms*—planar arrays, true-time-delay arrays, 3D beam training, spherical coverage efficiency, time-interleaving.**

I. Introduction

Fast beam acquisition is critical for success of next-generation wireless targeting high data rates at mmW frequencies but suffers from a fundamental trade-off between energy-efficiency and speed using mmW analog phased-array architectures relying on time-division-based beam sweeping [1], [2]. The need to estimate incident angles for both azimuth and elevation over 3D spaces further accentuate this problem challenging the spectral- and energy-efficiency of the network comprising several user elements (UE) served by single- or multiple base-stations (BS) as illustrated in Fig. 1.

Fast beam training which can sound all directions simultaneously using true-time-delay (TTD) arrays has been shown as an effective solution to overcome the large overhead in linear receiver arrays. The authors' prior works [3], [4] have demonstrated frequency dependent rainbow beams with unique frequency-to-angle map leveraging underlying waveform structure. This technique can simultaneously probe multiple directions efficiently in a single pilot symbol period using orthogonal frequency division multiplexing (OFDM) waveform overcoming fundamental limitations with beam probing in analog array architecture. However, expanding from a 2D space as demonstrated in [5] to a 3D space requires the array to steer antenna weights in both azimuth and elevation for the 3D beam training algorithm. This poses several hardware challenges that affect the overall end-to-end link latency as well as coverage efficiency and estimation accuracy. For example, an 8×8 array requires at least 2048 beams to achieve full spherical coverage within 1dB beamforming gain constraint as shown in [6].

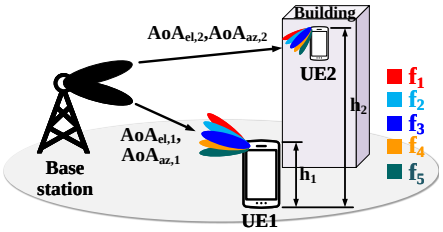

Fig. 1. Concept of the proposed frequency-dependent beamtraining algorithm over 3D space. AoA denotes angle-of-arrival.

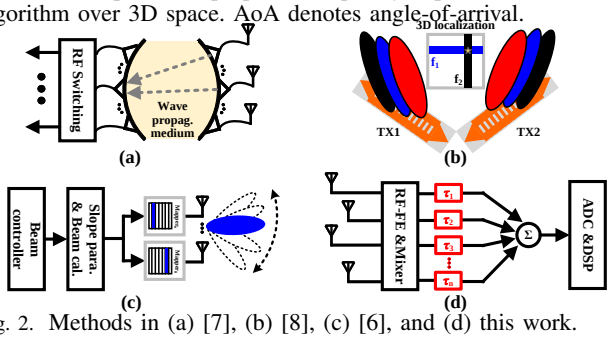

Fig. 2. Methods in (a) [7], (b) [8], (c) [6], and (d) this work.

Table I presents an overview of recent hardware implementations for 3D beam probing. Different methods to implement beamtraining are depicted in Fig. 2. In [7], a massive multi-input multi-output (MIMO) system was demonstrated using Rotman lens (Fig. 2(a)) to emulate frequency dispersion. However, construction complexity of the lens constrains its

This work was supported in part by NSF under grants 1955672, 1705026, and 1944688. This work was also supported in part by the ComSenTer and CONIX Research Centers, two of six centers in JUMP, a Semiconductor Research Corporation (SRC) program sponsored by DARPA.

Qiuyan Xu, Chung-Ching Lin, and Subhanshu Gupta are with the School of Electrical Engineering and Computer Science, Washington State University, Pullman, WA 99164 USA (e-mail: qiuyan.xu@wsu.edu).

Aditya Wadaskar, Han Yan, Veljko Boljanovic, and Danijela Cabric are with the Department of Electrical and Computer Engineering, University of California, Los Angeles, Los Angeles, CA 90095 USA (e-mail: adityaw@g.ucla.edu).

TABLE I
STATE-OF-THE-ART FOR 3D BEAMTRAINING

	[7]	[8]	[6]	This Work
Beam-probing	Yes (2D) No (3D)[1]	Yes (2D) Yes (3D)	Yes (2D) Yes (3D)	Yes (2D) Yes (3D)
# Chips	1	2	1	1
Method	Rotman lens	Leaky-wave antenna	Phase rotation + slope estimation	True-time delay
Freq. (GHz)	5	360-400	28	60 (emulation)
External Constructs[6]	Yes	Yes[2]	No	No
Multi-port Switching	Yes	No	Yes	No
Scalable / Compact	Low	Low[2]	High	High
Probing Time	NR	50 s–5ms[4]	3.4ms[3]	36.5 s[5]
Estimation RMSE	NR	NR	0:3 (Azi.) 0:26 (Elev.)[7]	0:13 (Azi.) 0:35 (Elev.)[7]

[1] Potential for 3D beam training; [2] Larger area and smaller aperture at lower carrier frequencies; [3] 8ns switching time and 200ns setup time in 256-element array; [4] Resolution BW 1/accuracy; [5] 100% coverage considering 446.25ns delay range and same switch/setup time as [6]; [6] For frequency dispersion; [7] 16 16 array with 16K beams (simulated).

scalability. In [8], leaky-wave antennas (LWAs) (Fig. 2(b)) were used to achieve beam training. However, the LWA size is strongly related to operating frequency, making the design bulky at lower frequencies. In [6], a 16; 384 beam codebook constructed using an 16×16 planar-phased array with fast switching (Fig. 2(c)) yields Root Mean Squared Error (RMSE) of $0{:}3^{\circ}$ and $0{:}26^{\circ}$ for the azimuth and elevation angles respectively, with a total beam-probing time of 3:4ms. In [9], beam training scanning of both azimuth and elevation planes was demonstrated at sub-THz using two ICs in azimuth and elevation respectively requiring an external LWA for each direction.

In this work, the authors extend the TTD approach in [4] to 3D beam training with the goal to realize equivalent spherical coverage using OFDM waveforms for ultra-fast training. The beam probing time and estimation accuracy are quantified as a function of TTD hardware design parameters including the time interleaving factor. For experimental system demonstration, the 2×2 planar TTD array (adopted from [5]) was used to demonstrate fast beam probing technique in 3D space using only a single IC as shown in Table I.

The rest of the paper is organized as follows. Section II provides insights of the 3D rainbow beam training algorithm. System architecture and implementation trade-offs are presented in Section III. Section IV contains the measured results and discussions followed by conclusions in Section V.

II. 3D BEAMTRAINING ALGORITHM USING TTD ARRAYS

We consider a uniform planar array with N antenna elements arranged in an $N_{az} \times N_{el}$ array, where N_{az} and N_{el} are the array dimensions. A 2D time delay network is deployed to generate frequency dependent probing beams. We consider uniformly spaced delay taps in each plane with spacings Δ_{az} and Δ_{el}. The cumulative delay at each antenna element is the sum of the delay components corresponding to the azimuth and elevation, *i.e.* $_{(n_{az};n_{el})} = _{az;n_{az}} + _{el;n_{el}}$. With uniformly

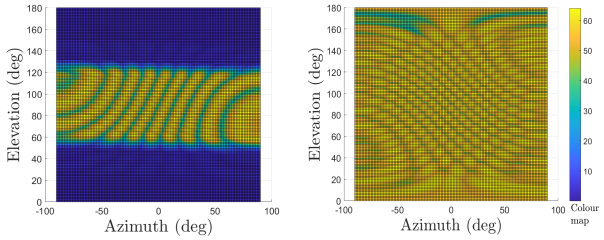

(a) 50% coverage (b) 100% coverage

Fig. 3. Total spatial footprint of 3D Rainbow beams, illustrated using a beam-forming gain heat-map, plotted on a 128×128 angle grid. $N_{az} = N_{el} = 8$, $f_c = 60GHz$, $BW = 6GHz$, $k_{opt} = 26$, $M_{sub} = 128$. (a) $b = 0{:}5$, $\Delta_{el} = 1{=}2\text{BW}$ (b) $b = 1$, $\Delta_{el} = 1{=}\text{BW}$.

spaced delay taps, we get $_{az;n_{az}} = (n_{az} - 1)\Delta_{az}$ and $_{el;n_{el}} = (n_{el}-1)\Delta_{el}$. The $(_{az};\ _{el})$ pair results in frequency dependent probing beams $\mathbf{w}(f) = \mathbf{w}_{az}(f) \otimes \mathbf{w}_{el}(f)$ mapped across the azimuth and elevation planes, and can be expanded using (4) in Table II.

Our goal is to design the delay spacings $(\Delta_{az}; \Delta_{el})$ and number of subcarriers M_{sub} used for beam training pilots to achieve full spherical coverage of codebook beams across the region of $_{az} \in [-\ {=}2;\ {=}2]$ and $_{el} \in [0;\ ]$. Full spherical coverage refers to the condition wherein codebook beams probe the entire angular space with sufficient beamforming gain, e.g. $(1 - \ )N$, where $\in (0; 1)$ is the beamforming gain constant and N is the maximum beamforming gain. Mathematically, spherical coverage efficiency is defined as the ratio of the continuous solid-angular region given by $\mathcal{A} = \left\{ (_{az};\ _{el}) \left| \max_f G(_{az};\ _{el}; f) \geq (1 - \ )N \right. \right\}$, and the total target solid-angular region of 2 , and is expressed as:

$$_{cov} = \frac{1}{2} \iint_{(_{az};\ _{el}) 2A} \sin\ _{el} d\ _{el} d\ _{az} \qquad (1)$$

where, $G(_{az};\ _{el}; f)$ is the beamforming gain as a function of the incident angle pair $(_{az};\ _{el})$ and frequency f.

Low-latency 3D beamtraining: The goal of the beamtraining algorithms is to quickly estimate dominant channel propagation path determined by $(_{az};\ _{el})$. Assuming the OFDM based training pilots, the received signal at subcarrier m is given by $Y[m] = \mathbf{w}^H(f_m)\mathbf{H}(f_m)\mathbf{v}X[m] + \mathbf{w}^H(f_m)\mathbf{n}(f_m)$, where $\mathbf{v} \in \mathbb{C}^{N_T}$ is the transmit beamforming precoder (known apriori), $X[m]$ denotes the non-zero unit-power-constrained beamtraining pilots at the subcarrier m, and $\mathbf{H}(f_m)$ is the channel matrix for subcarrier frequency f_m.

The planar array response $\mathbf{a}(_{az};\ _{el}; f)$ is given by the kronecker product of the array responses associated with the azimuth and elevation planes described in Table II (3): $\mathbf{a}(_{az};\ _{el}; f) = \mathbf{a}_{az}(_{az};\ _{el}; f) \otimes \mathbf{a}_{el}(_{el}; f)$. The beamforming gain is given by $G(_{az};\ _{el}; f) = |\mathbf{w}^{\mathrm{H}}(f)\mathbf{a}(_{az};\ _{el}; f)|^2$ and can be expressed as the product of beamforming gain functions in the azimuth and elevation planes: $G_{az}(_{az};\ _{el}; f)$ and $G_{el}(_{el}; f)$ respectively.

Based on our analysis in [10], a planar TTD array with $\Delta_{el} = \frac{b}{\mathrm{BW}}$ for coverage factor $b \in (0; 1]$, $\Delta_{az} = k\Delta_{el}$, where k, M_{sub} are chosen in accordance with (5) and (6) can realize a 3D beam codebook that scans the angular range $_{az} \in [-\frac{}{2}; \frac{}{2}]$ and $_{el} \in [\frac{}{2}(1-b);\ -\frac{}{2}(1-b)]$ at once, or in other words, achieves $(100 \times b)\%$ coverage efficiency. Fig. 3 illustrates the spatial occupancy of codebook beams

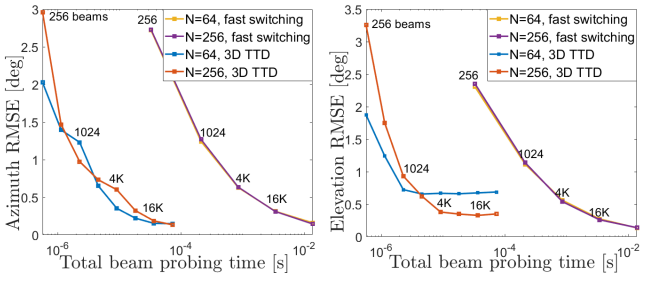

(a) Azimuth RMSE (b) Elevation RMSE

Fig. 4. Theoretical AoA RMSE achieved by fast-switching based phased-planar array codebook and 3D-TTD codebook, plotted against total beaam-probing time, for 8 8 and 16 16 array. (BW = 800MHz, k = 6:24 N_{el})

in the 3D angular space under 50% coverage ($b = 0.5$), where the elevation angles probed are restricted to [=4; 3 =4], and under 100% coverage ($b = 1$), where the entire 3D angular space is probed. The optimal value of k that ensures sufficient beam-proximity along the elevation plane depends only on the array geometry and elevation-plane beamforming gain constant $_{el} \in (0; 1)$, not on the target coverage efficiency. Table II describes a dictionary based 3D beamtraining algorithm to estimate the dominant AoA pair by correlating received signal power with the dictionary matrix described in (7). The 3D codebook design and proposed beamtraining procedure described above is backward compatible with 2D beamtraining.

Maximum delay range: The maximum delay range required by the planar array is the time delay applied to the $(N_{az}; N_{el})^{th}$ array element, given as follows.

$$\Delta t_{max} = (N_{el} - 1)\frac{b}{\text{BW}} + (N_{az} - 1)\frac{kb}{\text{BW}} \tag{2}$$

Using (2), a 2×2 planar TTD array with $k = 4.2$ (from (5)) requires a delay range of 6.5ns to achieve 100% coverage, and 3.75ns to achieve 50% coverage, when using bandwidth 800MHz, and $_{el} = _{az} = 0.5$.

Extension to larger arrays (8×8 or 16×16) is highly desirable to facilitate long range communication, thereby requiring large number of beams to probe the entire angular space owing to narrow beams. An 8×8 array requires at least 624 beams to achieve full spherical coverage with 3dB beamforming gain constraint. Increasing the number of beams further improves the AoA estimation accuracy owing to decreased beam-separation along the azimuth. On the other hand, increasing the ratio k improves the elevation angle estimation accuracy. Due to the limited number of subcarriers per OFDM symbol and unique frequency-angle mapping, implementing a dense high-resolution codebook of frequency-dependent beams requires multiple OFDM symbols and codebook rotations. Rotations are implemented using a phase shifting approach and do not require any additional delay adjustment.

An 8×8 TTD-planar array can implement 16; 384 frequency dependent beams spanning 8 OFDM symbols to yield theoretical AoA RMSE (0.18° and 0.67° for azimuth and elevation angles respectively) with total beam-probing time of 36.48 s, and delay range requirement of 446.25ns under 3dB beamforming gain constraint, when using bandwidth 800MHz. Fig. 4 illustrates the advantage of 3D-TTD-codebook based beam-probing over the fast-switching based planar array codebook proposed in [6], where the former is seen to achieve comparable theoretical AoA RMSE estimates to the latter with significantly reduced total beam-probing time. More elements help with RMSE but require larger beam probing time. Realizing the requisite bandwidth and delay range, however, pose a big design challenge to TTD IC design to be discussed next.

TABLE II
3D TTD BASED BEAMTRAINING

Array response & TTD combiner	*(d:element spacing, c:speed of light)*
1.	$[\mathbf{a}_{az}(\ _{az};\ _{el}; f)]_{n_{az}} = e^{(\ j\ (n_{az}\ \ 1)df \sin\ _{az} \sin\ _{el})=c}$ $[\mathbf{a}_{el}(\ _{el}; f)]_{n_{el}} = e^{(\ j\ (n_{el}\ \ 1)df \cos\ _{el})=c}$ (3)
2.	$[\mathbf{w}_x(f)]_{n_x} = \exp(j2\ f(n_x\ \ 1)\ \ _x);\ x = fazjelg$ (4)
Beam-widths	$(\ ; N)$
1.	$(\ _{az}; N_{az})$: azimuth-plane width of angular region satisfying $G_{az}(\ _{az}\ _{el}; f)\ \ (1\ \ _{az})N_{az}$ w.r.t. constant $_{az}$
2.	$(\ _{el}; N_{el})$: elevation-plane width of angular region satisfying $G_{el}(\ _{el}; f)\ \ (1\ \ _{el})N_{el}$ w.r.t. constant $_{el}$
3.	: Overall gain constant $G(\ _{az}\ _{el}; f)\ \ (1\ \ )N$
4.	$(1\ \ _{az})(1\ \ _{el})\ \ (1\ \ )$
3D Rainbow beam codebook design	
	For $(100\ \ b)\%$ *spherical coverage, where* $b\ \ 1$.
1.	$_{el} = \frac{b}{\text{BW}}$; $_{az} = \frac{2}{\Omega(\ _{el}; N_{el})}\ \ _{el}$; $k = \frac{2}{\Omega(\ _{el}; N_{el})}$ (5)
2.	$M_{sub} = \left\lceil \frac{4\ \Delta\ _{el}\ \text{BW}}{\Omega(\ _{el}; N_{el})\Omega(\ _{az}; N_{az})} \right\rceil$ (6)
3D Beamtraining algorithm	
1.	Generalised beamforming gain dictionary: $\mathbf{B}\ 2\ \mathbb{R}^{M_{sub}\ \ Q_a Q_e}$ $[\mathrm{B}]_{m;i} = \left\lvert \mathbf{w}^H(f_m)\mathbf{a}\left(\begin{smallmatrix}{}_{az};\ {}_{el}\\ {}_{a(i)};\ {}_{e(i)}; f_m\end{smallmatrix}\right)\right\rvert^2$ (7) Q_a azimuth $\angle$ candidates $_a$, $a = 1; :::; Q_a$ Q_e elevation $\angle$ candidates $_e$, $e = 1; :::; Q_e$. $a(i) = i\ \ \left\lfloor \frac{i}{Q_a} \right\rfloor$, $e(i) = \left\lfloor \frac{i}{Q_a} \right\rfloor + 1$; $m\ 2\ M, jMj = M_{sub}$
2.	Power at subcarrier m: $\hat{\mathbf{p}}[m] = jY[m]j^2$
3.	**Estimated AoA:** $\left(\hat{}_{az}; \hat{}_{el}\right) = \left\{ \begin{smallmatrix}{}_{az}\\ (q^*\ \ \lfloor \frac{q^*}{Q_a} \rfloor)\end{smallmatrix};\ \begin{smallmatrix}{}_{el}\\ (\lfloor \frac{q^*}{Q_a} \rfloor + 1)\end{smallmatrix} \right\}$ where $q\ = \arg\max_q \frac{\hat{\mathbf{p}}^T[\mathbf{B}]_{:;q}}{k[\mathbf{B}]_{:;q}k}$

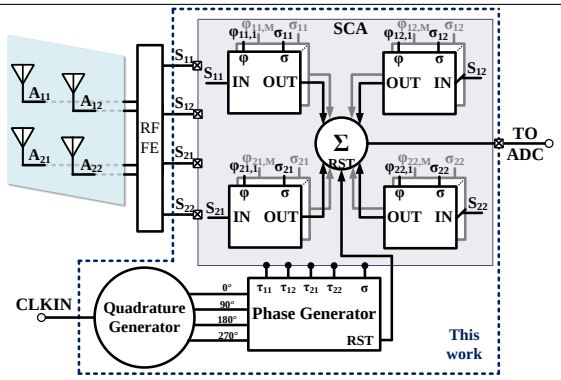

Fig. 5. 2×2 array system [5]. RF front-end (RF FE) is not included.

III. Proposed System Implementation

This section describes the system architecture briefly followed by key design considerations to enable beamtraining.

System architecture: A simplified system architecture to evaluate the efficacy of 3D beamtraining is shown in Fig. 5 (adapted from [5]).A 2x2 TTD-array is implemented together with its phase generator. Figure 6 presents the system timing diagram where the input clock is split in quadrature phases and then interleaved to generate different reference clocks. $_{11...22}$; $_{11...22}$ and RST are non-overlapping clock phases for sampling, summation and reset respectively enabling element-wise delay compensation on each of the four received chan-

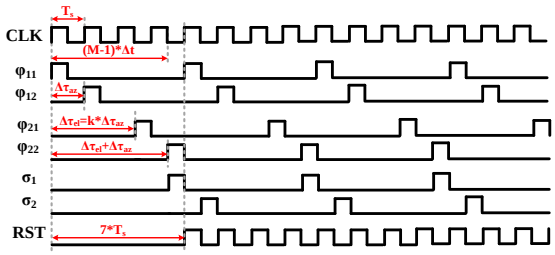

Fig. 6. Timing diagram of a 2×2 array.

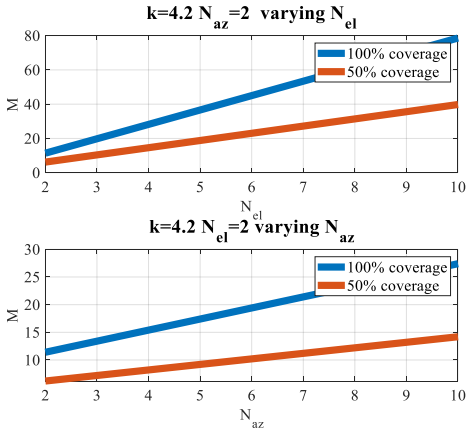

Fig. 7. Required interleaving factor, M against spherical coverage and number of elements in azimuth (N_{az}) and elevation (N_{el}).

nels. The summer combines the delay compensated and phase-shifted signals producing a single beamformed output.

Interleaving factor: Using interleaved clock phases as sampling clocks in different channels is equivalent to delaying the desired signal as proved in [11] enabling realization of large delay ranges. The clock interleaving factor is one of the most important parameters in realizing maximum achievable delay and is analyzed for 3D beam training. As interleaving factor increases, the system can have larger maximum delay with more non-overlapping phases. In [11], the interleaving factor is discussed for a linear TTD array. Similar to [11], for a 3D setup with planar TTD arrays, the minimum interleaving factor M is determined as follows:

1) Using (2), the maximum compensation delay $T_{C,max}$ achieved by the discrete-time TTD beamformer with an interleaving factor of M is:
$$T_{C,max} = (M-1) \times T_s \tag{8}$$
where T_s is the sampling period. To satisfy Nyquist criterion, $T_s \leq 1$=2BW.
2) Combining (2) and (8), M can be obtained as:
$$\frac{b(N_{az}-1)}{BW} + \frac{b(N_{el}-1)\times k}{BW} \leq (M-1)\times T_s \leq \frac{b(M-1)}{2\cdot BW} \tag{9}$$
$$M \geq 2(N_{az}-1) + 2(N_{el}-1)\cdot k + 1 \tag{10}$$

Figure 7 shows M against N_{az} and N_{el} as a function of optimal ratio k for different coverage efficiency when performing 3D beamtraining. To achieve a 100% ($b = 1$) coverage efficiency, M is required to be doubled compared to 50% ($b = 0{:}5$) coverage case. Larger number of elements in azimuth and elevation direction will further require M to increase. However, as observed in Fig. 7, M changes more rapidly with changing N_{el} due to the optimal ratio k.

In this work, a 2×2 array with $k = 4{:}2$ aiming 50% coverage efficiency requires the interleaving to be 6.2 (rounded

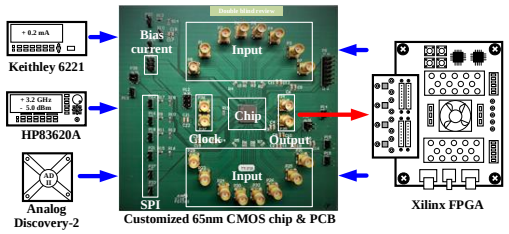

Fig. 8. Experimental system test setup (adapted from [5]).

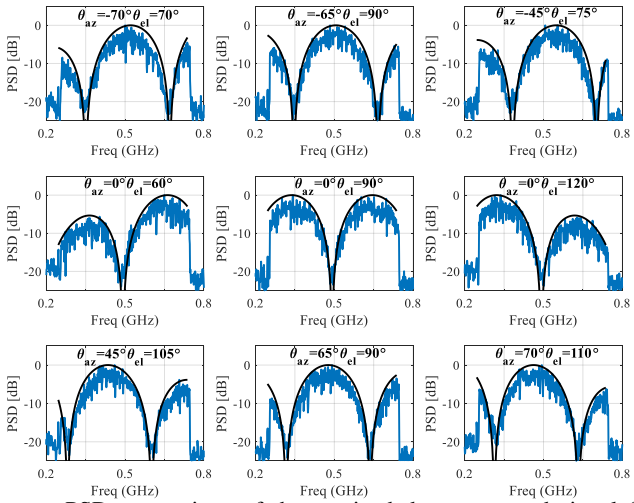

Fig. 9. PSD comparison of the received downconverted signal for different AoA using 2×2 TTD SSP. (Blue) Measured PSD. (Black) Theoretical PSD estimated from eqn. (7) in Table II.

to 7). It is also worth noting that the signal bandwidth does not directly affect M. This is because as the bandwidth increases, the sampling frequency needs to increase accordingly to meet the Nyquist criterion. However, it does not imply an unconstrained bandwidth expansion.

IV. Measurement Results

The system testbed setup for 3D beamtraining is shown in Fig. 8 and comprises of the Xilinx ZCU216 RFSoC with 16-channel synchronized GS/s RF-DACs as arbitrary waveform generator, signal generator for master clock generation (HP83620A), and Analog Discovery II to communicate with the on-chip serial-to-parallel interface (SPI). The TTD SSP adapted from [5] is fabricated in 65nm CMOS technology and packaged in a 72-pin Quad Flat No-leads (QFN) package that is mounted on the PCB for verification.

To facilitate the test procedure, computer-vision based techniques are applied to automate the DUT characterization with the Xilinx ZCU216 RFSoC in closed-loop. The automation uses Python scripting and MATLAB for different tasks including generation of different OFDM symbols, data collection, and post-processing. Each generated OFDM symbol in MATLAB emulates different incident azimuth $_{az}$ and elevation angles $_{el}$ and represents 800MHz bandwidth assumed to be downconverted from mmW (60GHz) to IF (491:32MHz) at 960kHz carrier spacing and antenna spacing of 2.5mm. In absence of over-the-air synchronization, the single OFDM symbol repeats itself in these experiments.

Figure 9 compares the measured power spectral density (PSD) with the theoretical PSD where different $_{el}$ and $_{az}$ are applied. The input azimuth angle sweeps from -70 to 70

Fig. 10. Heatmap of measured PSD for different $_{el}$ and $_{az}$. (Black dot) - measured peak of likelihood in the AoA estimation; (Red dot) - ground truth AoA peak values (q* in equation (7) Table II).

and input elevation angle sweeps from 60 to 120 . It can be observed that the PSD plot is unique and closely matches to the theoretical estimates based on (7) in Table II.

Figure 10 provides a more intuitive comparison of the measured PSD. In special cases where $_{el} = 90$ and/or $_{az} = 0$, the 3D array degenerates to a linear array since the incidence beam is always parallel to horizontal axis or vertical axis respectively. Consider the case where $_{el} = 90$, it is equivalent to a 2D beamtraining with incidence angle of $_{az}$. Similarly, if $_{az} = 0$, it can be seen as a linear array with $= _{el}$. In general, each output PSD should be unique in peak/squint amplitude and/or frequency for different incidence $_{el}$ and $_{az}$. Nine specific cases are shown with each of them being identical in peak/squint value and/or frequency. The PSD plots should be symmetric for dual input pairs. For example, $_{el} = 70\ ;\ _{az} = -70$ is symmetric to $_{el} = 110\ ;\ _{az} = 70$, and $_{el} = 90\ ;\ _{az} = -65$ is symmetric to $_{el} = 90\ ;\ _{az} = 65$. In most cases the angle estimation error is within 10 , and two input pairs $_{el} = 70\ ;\ _{az} = -70$ and $_{el} = 90\ ;\ _{az} = -65$ have an estimation error close to 10 . Based on the predicted and measured results, a rainbow codebook could thus be established to realize fast beamtraining over 3D space.

V. Conclusions

This work shows the first demonstrated single-chip low-latency 3D beamtraining algorithm for analog arrays leveraging cross-system design methodology based on TTD arrays. Detailed considerations of 3D frequency-dependent beamtraining algorithm codesign with underlying TTD hardware is presented considering delay ranges and spherical coverage efficiencies. Supporting experiments on a proof-of-concept 2×2 prototype accurately estimate the incident azimuth and elevation angles with 50% coverage efficiency over 800MHz bandwidth and 3.75ns delay range. The prototype fabricated in 65nm CMOS occupies an area of 1.98mm^2 consuming 29mW power. Finer resolution, larger spherical coverage efficiency and bandwidths can be expected for future designs leading to development of integrated 3D beamtraining and beamforming communication systems.

References

[1] M. Giordani, M. Polese, A. Roy, D. Castor, and M. Zorzi, "A tutorial on beam management for 3GPP NR at mmWave frequencies," *IEEE Communications Surveys Tutorials*, vol. 21, no. 1, pp. 173–196, 2019.

[2] Z. Marzi, D. Ramasamy, and U. Madhow, "Compressive channel estimation and tracking for large arrays in mm-Wave picocells," *IEEE Journal of Selected Topics in Signal Processing*, vol. 10, no. 3, pp. 514–527, 2016.

[3] V. Boljanovic, H. Yan, E. Ghaderi, D. Heo, S. Gupta, and D. Cabric, "Design of millimeter-wave single-shot beam training for true-time-delay array," in *2020 IEEE 21st International Workshop on Signal Processing Advances in Wireless Communications (SPAWC)*, 2020, pp. 1–5.

[4] V. Boljanovic, H. Yan, C.-C. Lin, S. Mohapatra, D. Heo, S. Gupta, and D. Cabric, "Fast beam training with true-time-delay arrays in wideband millimeter-wave systems," *IEEE Transactions on Circuits and Systems I: Regular Papers*, vol. 68, no. 4, pp. 1727–1739, 2021.

[5] C.-C. Lin, C. Puglisi, E. Ghaderi, S. Mohapatra, D. Heo, S. Gupta, H. Yan, V. Boljanovic, and D. Cabric, "A 4-element 800MHz-BW 29mW true-time-delay spatial signal processor enabling fast beam-training with data communications," in *ESSCIRC 2021 - IEEE 47th European Solid State Circuits Conference (ESSCIRC)*, 2021, pp. 287–290.

[6] B. Sadhu, A. Paidimarri, W. Lee, M. Yeck, C. Ozdag, Y. Tojo, J.-O. Plouchart, X. Gu, Y. Uemichi, S. Chakraborty, Y. Yamaguchi, N. Guan, and A. Valdes-Garcia, "A 24-to-30GHz 256-element dual-polarized 5G phased array with fast beam-switching support for >30,000 beams," in *2022 IEEE International Solid- State Circuits Conference (ISSCC)*, vol. 65, 2022, pp. 436–438.

[7] Y. Gao, M. Khaliel, F. Zheng, and T. Kaiser, "Rotman lens based hybrid analog–digital beamforming in massive MIMO systems: Array architectures, beam selection algorithms and experiments," *IEEE Transactions on Vehicular Technology*, vol. 66, no. 10, pp. 9134–9148, 2017.

[8] H. Saeidi, S. Venkatesh, X. Lu, and K. Sengupta, "THz Prism: One-shot simultaneous localization of multiple wireless nodes with leaky-wave THz antennas and transceivers in CMOS," *IEEE Journal of Solid-State Circuits*, vol. 56, no. 12, pp. 3840–3854, 2021.

[9] H. Saeidi, S. Venkatesh, X. Lu, and K. Sengupta, "22.1 THz Prism: One-shot simultaneous multi-node angular localization using spectrum-to-space mapping with 360-to-400GHz broadband transceiver and dual-port integrated leaky-wave antennas," in *2021 IEEE International Solid-State Circuits Conference (ISSCC)*, vol. 64, 2021, pp. 314–316.

[10] A. Wadaskar, V. Boljanovic, H. Yan, and D. Cabric, "3D Rainbow beam design for fast beam training with true-time-delay arrays in wideband millimeter-wave systems," in *2021 55th Asilomar Conference on Signals, Systems, and Computers*, Nov. 2021, pp. 1–4.

[11] E. Ghaderi, A. Sivadhasan Ramani, A. A. Rahimi, D. Heo, S. Shekhar, and S. Gupta, "An integrated discrete-time delay-compensating technique for large-array beamformers," *IEEE Transactions on Circuits and Systems I: Regular Papers*, vol. 66, no. 9, pp. 3296–3306, 2019.